Universal computing by DNA origami robots in a living animal

Published in final edited form as:
Nat Nanotechnol. 2014 May ; 9(5): 353–357. doi:10.1038/nnano.2014.58.

Universal computing by DNA origami robots in a living animal

Yaniv Amir[#1], **Eldad Ben-Ishay**[#1], **Daniel Levner**[2], **Shmulik Ittah**[1], **Almogit Abu-Horowitz**[1], and **Ido Bachelet**[1,3]

[1]Faculty of Life Sciences and the Institute of Nanotechnology & Advanced Materials, Bar-Ilan University, Ramat Gan, Israel

[2]Wyss Institute for Bio-Inspired Engineering, Harvard Medical School, Boston, MA, USA

[#] These authors contributed equally to this work.

Abstract

Biological systems are collections of discrete molecular objects that move around and collide with each other. Cells carry out elaborate processes by precisely controlling these collisions, but developing artificial machines that can interface with and control such interactions remains a significant challenge. DNA is a natural substrate for computing and has been used to implement a diverse set of mathematical problems[1-3], logic circuits[4-6] and robotics[7-9]. The molecule also naturally interfaces with living systems, and different forms of DNA-based biocomputing have previously been demonstrated[10-13]. Here we show that DNA origami[14-16] can be used to fabricate nanoscale robots that are capable of dynamically interacting with each other[17-18] in a living animal. The interactions generate logical outputs, which are relayed to switch molecular payloads on or off. As a proof-of-principle, we use the system to create architectures that emulate various logic gates (AND, OR, XOR, NAND, NOT, CNOT, and a half adder). Following an ex vivo prototyping phase, we successfully employed the DNA origami robots in living cockroaches (Blaberus discoidalis) to control a molecule that targets the cells of the animal.

To implement a collision-based computer using DNA objects, we used the DNA origami nanorobots described previously[19] (Supplementary Note 1). These robots are controlled by a gate that opens in response to a correct combination of protein cues, which bind a sensing strand, typically an aptamer, and displace it from its complementary strand. Upon displacing the gate strands from each other the robot undergoes a drastic conformational shift, exposing the payload inside it and making it available to engage target cells. Here, these payloads mediate and control collisions between robots as described below.

In our design, the gate can be opened also by an external DNA key, which hybridizes with the complementary strand in the gate, displacing the sensing strand by toehold-mediated migration[17-18] and activating the robot. This DNA key can now be mounted as payload into one robot, such that when this robot is active, the strand can access the gate of an adjacent robot, subsequently altering its state to active as well. This assigns a “positive regulator” (P)

[3]Correspondence and requests for materials should be addressed to Ido Bachelet, Faculty of Life Sciences, Bar-Ilan University, Ramat Gan 52900, Israel. Tel/Fax: +972 3 738 4312. ido.bachelet@biu.ac.il.
Author contribution: All authors designed experiments; Y.A., E.B.I, S. I., A.A.H. and I.B. performed experiments; all authors wrote the manuscript.

Europe PMC Funders Author Manuscripts

phenotype to the robot loaded with the external key. A “negative regulator” (N) phenotype can be assigned as well: here, the first robot is loaded with DNA clasps that cross-link two juxtaposed sides of the second robot’s gate, forcing it to close or preventing it from becoming open. These dynamic DNA interactions were designed and simulated using visual DSD[20] (Supplementary Note 2).

We designed various architectures by mixing P and N robots with effector (E) robots at defined ratios in the presence or absence of their cognate protein cues. To demonstrate this platform in a living biological system, we used living adult *Blaberus discoidalis* as model organisms. We found this animal to be an excellent model for initial prototyping of DNA nano-devices for its very low systemic nuclease activity, small systemic volume, and chemical compatibility with DNA structures. After loading E robots with an antibody recognizing the insect’s hemocytes (the hemolymph cells analogous to human white blood cells), robot mixtures were tested on freshly isolated hemocytes and then injected into the living animals (Supplementary Notes 3 and 4).

We first tested E robots controlled by a gate that opens if and only if both cues (termed X and Y) are present. E robots alone (which we call an E architecture) emulate a logical AND gate (Fig. 1A & Supplementary Fig. 15) as previously described[19].

We next added two robot types, P1 (opens in response to X and carries a single key to the Y gate of E) and P2 (opens in response to Y and carries a single key to the X gate of E). Adding P1 and P2 to E (EP1P2 architecture) enables E to open in response to X alone (by P1), Y alone (by P2), or XY (by itself), emulating a logical OR gate (Fig. 1A & Supplementary Fig. 16). Binding of target cells by an EP1 or EP2 robot complex instead of just E robots was shown by tagging P1 and P2 with fluorophores, resulting in fluorescence intensity patterns clearly indicating the presence of EP complexes (Supplementary Fig. 17). It is important to note that an OR gate can be achieved more simply using 1 or 2 robot types; however, 3 robots have a higher capacity for molecular control (3 therapeutic molecules instead of 2). We observed no significant change in speed or error rate when moving from 2 to 3 robots in this configuration.

We then added N robots (EP1P2N architecture), N being activated if and only if both X and Y are present. Here, in contrast to EP1P2, the presence of both X and Y activates N, which carries multiple clasp arms that close E, subsequently negating or preventing E activation (importantly, the N clasps cannot hybridize with the N gates themselves). These outputs are identical to the ones generated by a XOR gate. In the final state of the EP1P2N architecture, E is always in complex with P1 or P2 (when it is active) or N (when it is inactive). XOR was successfully emulated only when N was at a molar excess of 10 over E (Fig. 1A & Supplementary Fig. 18).

E robots in EP1P2N generate XOR, while N robots in this architecture generate AND, together enabling the construction of a half adder, in which the sum bit is relayed by E and the carry bit by N. Hence, it can be programmed to respond to a cue count rather than to the identity of particular cues. However, both robot types in the EN complex (unlike in the EP complexes) directly face each other and therefore utilizing N to deliver a payload is

sterically inhibited; however, the carry bit can be utilized by adding a second effector robot (F), which is not keyed by P1 and P2 and is not negated by N. Thus, either X or Y alone activate E, while XY together activate only F (E being negated by N). P1 and P2 cannot key F because the toeholds extending from the F gates are different from the ones on the E gates. Moreover, N cannot negate F because F gates lack the additional extensions that enable N arms to clasp them together (Supplementary Note 2). The half adder adder (EFP1P2N) functioned well at a stoichiometry of 1:1:5:5:10 (Fig. 1A,C). This stoichiometric hierarchy was highly consistent with the predictions made in vDSD as to the EP and EPN collisions.

We introduced a modified type of E, termed E_{open}, which is similar to E but lacks sensing strands (thus it is constitutively open regardless of the inputs X and Y). E_{open}N architecture, made by mixing E_{open} with N, produces 0 in response to XY, and 1 otherwise, like the NAND gate (Fig. 2a & Supplementary Fig. 19). An inverter (NOT) can be readily designed as a variant of the NAND gate, constructed by programming N to respond only to X (by placing two identical X gates instead of X and Y gates on the robot), termed N_X. E_{open}:N_X architecture produces 1 if X is absent (by E_{open}) and 0 if X is present (by N_X negating E_{open}) (Fig. 2b).

Architectures based on more than one effector robot (like the EFP1P2N mentioned above) can relay output bits to additional therapeutic molecules, forming the basis for more complex gates, reversible logic and binary decoders. To demonstrate this, a controlled NOT (CNOT) gate was designed, consisting of E, P1, P2 and N as described above, and in addition a second effector robot, F, not negated by N, and a positive regulator robot P3 that responds only to X and keys only F. Thus, one input bit is XORed by E and the second input bit is mapped unchanged by F. The CNOT gate (EFP1P2P3N) functioned well at a 1:1:5:5:5:10 stoichiometry (Fig. 3, see also Supplementary Table 1 for a summary of the outputs and effector complexes exerting them in the various architectures designed in this study).

The performance of our system and similar ones depends on the ability of its parts to freely interact. We used fluorescence correlation spectroscopy to measure robot diffusion in a medium mimicking the fluid mechanical properties of the insect's hemolymph (Supplementary Note 5, Supplementary Fig. 26), yielding a diffusion coefficient of 19±1.1 μ^2/s at the open state and 21±2.6 μ^2/s at the close state. Typically, 0.1-3 pmol robots interact within an average hemolymph volume of 650 μL (assuming total cell volume is negligible). While in this space and medium sheer diffusion would not likely support efficient collisions in reasonable time scales (Supplementary Fig. 27), the insect hemolymph is constantly mixed. *Periplaneta americana*, closely related to *B. discoidalis*, has a heart rate of 130±10 beats/min with an average stroke volume of 1.9±0.31 μL, resulting in a cardiac output equivalent to 38% of the hemolymph volume per minute, providing for efficient computing as observed here. The estimated Reynolds number of the insect's open circulatory system is in the order of 1-5 due to the low-velocity flow within the small hemocoel[21]. Compared to that, Reynolds numbers in the human circulatory system range from 1 in arterioles to ~4,000 in the aorta and vena cava. Therefore, our study shows that computing in human blood should be at least as efficient as that observed in the insect model. Scaling the system to humans would require increasing robot quantity by ~4 orders of magnitude, and constructing

them using nuclease-resistant analogues such as LNA. These essentially technical issues should be achievable in the very near future.

The architectures described here are capable of processing two input bits at most. However, the outputs from two “processors” can be relayed to a third one and increase the processing capacity, which would be limited by the possible number of unique gate-key systems that can be designed. Importantly, the scaling of our design is linear rather than logarithmic, with errors in robot activation propagating in the order of the root sum square of the number of unique robot types in a system (Supplementary Note 6). Fig. 4 shows a schematic of a hypothetic 4-bit architecture for an imaginary task of controlling 3 therapeutic molecules simultaneously, although only the number of robots comprising the system limits its capacity. The basic concept we describe can be scalable plausibly to exceed the capacity of older 8-bit computers such as Commodore 64 or Atari 800, which many of us had the pleasure of experiencing as children.

The system we described can also be used to retrieve biochemical and physiological information as a diagnostic tool. However, for this the original cues need to be explicitly inferred from the final states of all the robots comprising the system. This is not possible in gates such as AND, OR and XOR, as these lose 1 bit per operation. However, it is made possible in reversible logic[22], using operators such as the CNOT gate demonstrated here, in which every input bit is mapped to an output bit. This information could be analysed in various ways, for example monitoring fluorescent outputs associated with robot final states.

This work presents a new type of biological computing platform particularly fit for the task of controlling therapeutic molecules in living organisms. Further design work building on this concept could significantly improve the capacity and efficiency of such systems towards a working prototype for computational control of therapeutics and other biological processes in humans in the near future.

Methods summary

DNA origami Robots were designed using caDNAno 2.0 (http://caDNAno.org), and folded using M13mp18 ssDNA as scaffold strand in TAE buffer containing 10 mM magnesium. Robots were cleaned by gel filtration on Amicon Ultra 100K columns. DNA strand displacement interactions were designed and simulated using visual DSD. Robots were imaged using TEM and AFM, and their states were measured using flow cytometry. Adult *Blaberus discoidalis* were maintained at constant room temperature in humid plastic cages with dry pet food and fresh fruit ad libitum. Robots (typically 0.1-3 pmol in 10 uL buffer) were injected into the animal hemocoel between the two last abdominal sternites. Hemolymph was extracted through the arthrodial membrane and mixed with anticoagulant buffer before hemocytes analysis. For detailed methods see Supplementary Information.

Supplementary Material

Refer to Web version on PubMed Central for supplementary material.

Acknowledgments

We are extremely grateful to these colleagues for their valuable advice and comments on the manuscript: A. Adamatzky, S. Revzen, D. Y. Zhang, R. Jungmann, P. Yin, A. Marblestone, E. Shapiro, A. Munitz, A. Binshtok, L. Qian, E. Winfree and G. M. Church. We are particularly grateful to S. M. Douglas for valuable contributions. We thank all the members of the Bachelet lab at Bar Ilan University for support, technical help and valuable discussions. This work was supported by a Kamin grant from the Israeli Ministry of Industry & Commerce, and grants from the Faculty of Life Sciences and the Institute of Nanotechnology & Advanced Materials at Bar-Ilan University.

References

1. Adleman LM. Molecular computation of solutions to combinatorial problems. Science. 1994; 266:1021–1024. [PubMed: 7973651]
2. Braich RS, Chelyapov N, Johnson C, Rothemund PW, Adleman L. Solution of a 20-variable 3-SAT problem on a DNA computer. Science. 2002; 296:499–502. [PubMed: 11896237]
3. Qian L, Winfree E, Bruck J. Neural network computation with DNA strand displacement cascades. Nature. 2011; 475:368–372. [PubMed: 21776082]
4. Seelig G, Soloveichik D, Zhang DY, Winfree E. Enzyme-free nucleic acid logic circuits. Science. 2006; 314:1585–1588. [PubMed: 17158324]
5. Stojanovic MN, Mitchell TE, Stefanovic D. Deoxyribozyme-based logic gates. J. Am. Chem. Soc. 2002; 124:3555–3561. [PubMed: 11929243]
6. Stojanovic MN, et al. Deoxyribozyme-based ligase logic gates and their initial circuits. J. Am. Chem. Soc. 2005; 127:6914–6915. [PubMed: 15884910]
7. Andersen ES, et al. Self-assembly of a nanoscale DNA box with a controllable lid. Nature. 2009; 459:73–76. [PubMed: 19424153]
8. Lund K, et al. Molecular robots guided by prescriptive landscapes. Nature. 2010; 465:206–210. [PubMed: 20463735]
9. Muscat RA, Bath J, Turberfield AJ. A programmable molecular robot. Nano Lett. 2011; 11:982–987. [PubMed: 21275404]
10. Benenson Y, Gil B, Ben-Dor U, Adar R, Shapiro E. An autonomous molecular computer for logical control of gene expression. Nature. 2004; 429:423–429. [PubMed: 15116117]
11. Benenson Y, et al. Programmable and autonomous computing machine made of biomolecules. Nature. 2001; 414:430–434. [PubMed: 11719800]
12. Modi S, Nizak C, Surana S, Halder S, Krishnan Y. Two DNA nano machines map pH changes along intersecting endocytic pathways inside the same cell. Nat. Nanotechnol. 2013; 8:459–467. [PubMed: 23708428]
13. Rudchenko M, et al. Autonomous molecular cascades for evaluation of cell surfaces. Nat. Nanotechnol. 2013; 8:580–586. [PubMed: 23892986]
14. Douglas SM, et al. Self-assembly of DNA into nanoscale three-dimensional shapes. Nature. 2009; 459:414–418. [PubMed: 19458720]
15. Douglas SM, et al. Rapid prototyping of 3D DNA-origami shapes with caDNAno. *Nucleic Acids Res*.. 2009; 37:5001–5006. [PubMed: 19531737]
16. Rothemund PW. Folding DNA to create nanoscale shapes and patterns. Nature. 2006; 440:297–302. [PubMed: 16541064]
17. Zhang DY, Seelig G. Dynamic DNA nanotechnology using strand-displacement reactions. Nat. Chem. 2011; 3:103–113. [PubMed: 21258382]
18. Zhang DY, Winfree E. Control of DNA strand displacement kinetics using toehold exchange. J. Am. Chem. Soc. 2009; 131:17303–17314. [PubMed: 19894722]
19. Douglas SM, Bachelet I, Church GM. A logic-gated nanorobot for targeted transport of molecular payloads. Science. 2012; 335:831–834. [PubMed: 22344439]
20. Lakin MR, Youssef S, Polo F, Emmott S, Phillips A. Visual DSD: a design and analysis tool for DNA strand displacement systems. Bioinformatics. 2011; 27:3211–3213. [PubMed: 21984756]

21. Lee WK, Socha JJ. Direct visualization of hemolymph flow in the heart of a grasshopper (S. americana). BMC Physiol. 2009; 9:2. [PubMed: 19272159]
22. Liu D, et al. Resettable, multi-readout logic gates based on controllably reversible aggregation of gold nanoparticles. Angew. Chem. Int. Ed. Engl. 2011; 50:4103–4107. [PubMed: 21452185]
23. Green LS, et al. Inhibitory DNA ligands to platelet-derived growth factor B-chain. Biochemistry. 1996; 35:14413–14424. [PubMed: 8916928]
24. Kaur H, Yung LY. Probing high affinity sequences of DNA aptamer against VEGF165. PLoS One. 2012; 7:e31196. [PubMed: 22359573]
25. Castro CE, et al. A primer to scaffolded DNA origami. Nat. Methods. 2011; 8:221–229. [PubMed: 21358626]
26. Bulmer MS, Bachelet I, Raman R, Rosengaus RB, Sasisekharan R. Targeting an antimicrobial effector function in insect immunity as a pest control strategy. Proc. Natl. Acad. Sci. USA. 2009; 106:12652–12657. [PubMed: 19506247]
27. Garbutt JS, Belles X, Richards EH, Reynolds SE. Persistence of double-stranded RNA in insect hemolymph as a potential determiner of RNA interference success: Evidence from Manduca sexta and Blattella germanica. J. Insect Physiol. 2013; 59:171–178. [PubMed: 22664137]
28. Magde D, Elson E, Webb WW. Thermodynamic fluctuations in a reacting system: measurement by fluorescence correlation spectroscopy. Phys. Rev. Lett. 1972; 29:705–708.
29. Korlann Y, Dertinger T, Michalet X, Weiss S, Enderlein J. Measuring diffusion with polarization-modulation dual-focus fluorescence correlation spectroscopy. Opt. Express. 2008; 16:14609–14616. [PubMed: 18794997]

Europe PMC Funders Author Manuscripts

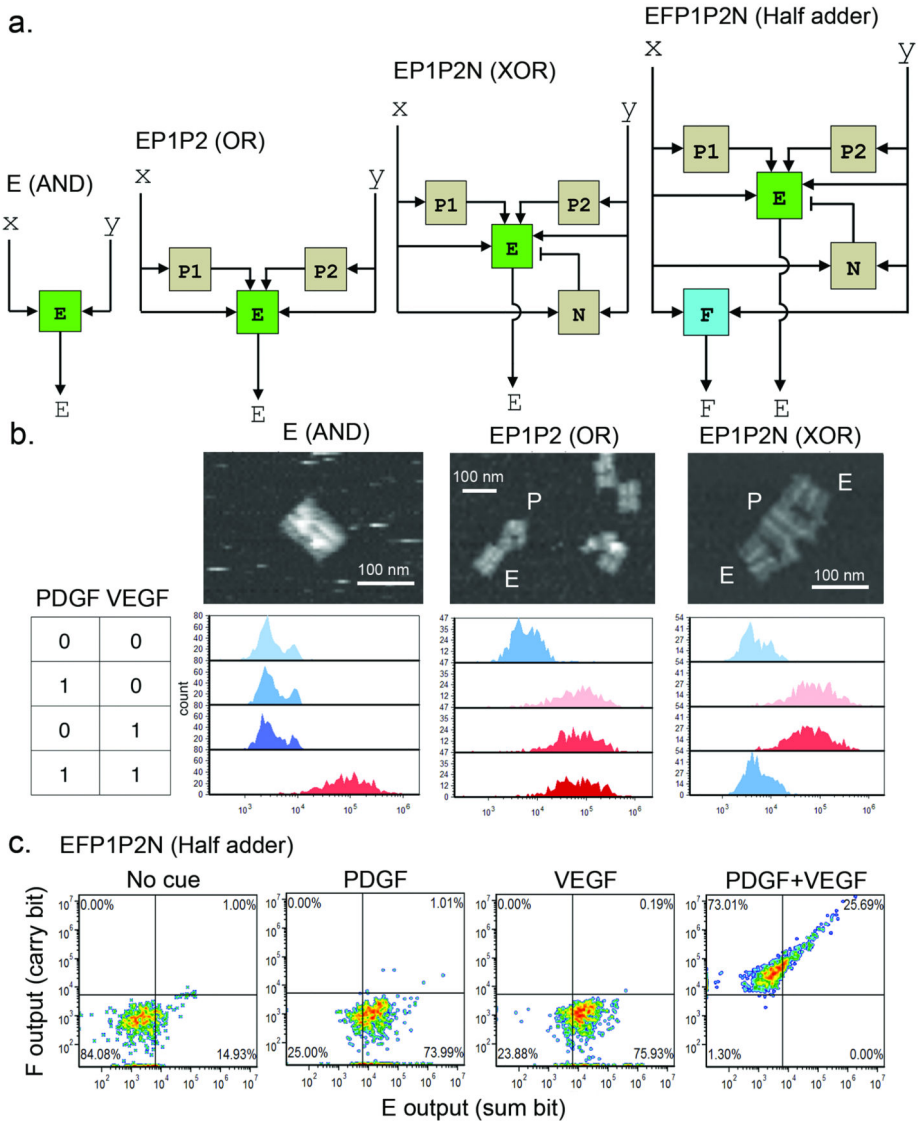

Fig. 1. Robots emulating AND, OR and XOR gates in a living animal.

A, schematic architecture representations. E robots (first from left) are equivalent to an AND gate, requiring both X and Y (in this study PDGF and VEGF, respectively) to open. EP1P2 architecture (second from left) functions as an OR gate, requiring either X, Y, or both to open. EP1P2N architecture (third from left) functions as a XOR gate, opening with either X or Y, but closing with both X and Y. EFP1P2N (right) emulates a half adder encoding the sum bit in E and carry bit in F. **B,** Top panels, AFM images (bars in nm) of robot architectures. Below every image is the corresponding flow cytometric analysis of insect cells isolated from *B. discoidalis* several hours following the injection of robots and appropriate keys. The table on the left shows key combination corresponding to each row of the histograms. E robots (FL1 channel) were tagged with FAM. Blue/red peaks represent negative/positive signals, respectively. **C**, flow cytometric analysis of the EFP1P2N architecture, emulating a half adder. E robots representing the sum bit (FL1 channel) and F robots (FL4 channel) representing the carry bit of the half adder were measured simultaneously in-vivo using FAM and Cy5 tagged robots. 1,000 hemocytes were collected for each experiment.

Europe PMC Funders Author Manuscripts

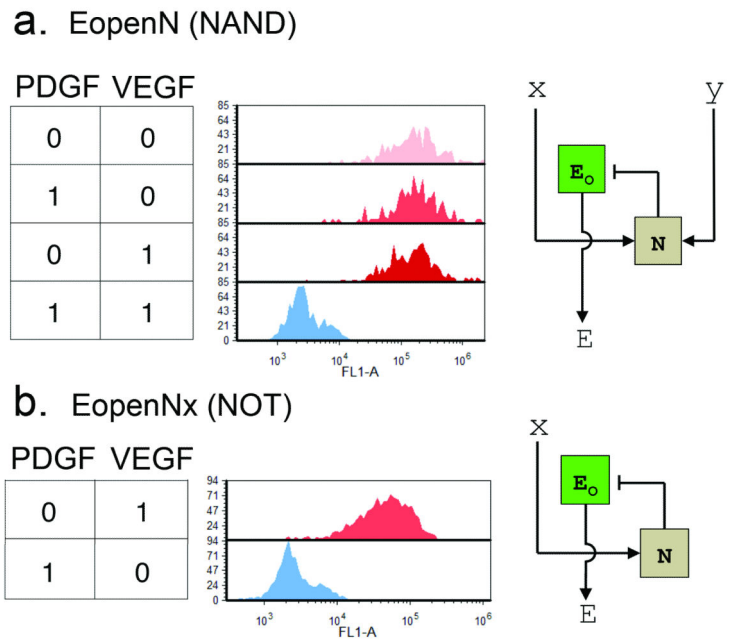

Fig. 2. Robots emulating NAND and NOT in a living animal.

A, The $E_{open}N$ architecture emulating the logically complete NAND gate. **B**, The $E_{open}N_X$ architecture emulating an inverter (NOT). Histograms are flow cytometric analysis of hemocytes extracted from *B. discoidalis* following injection of the proper robot architectures with keys. The table on the left shows key profile corresponding to each row of the histograms. Below are schematic representations of robot architectures. 1,000 hemocytes were collected for each experiment.

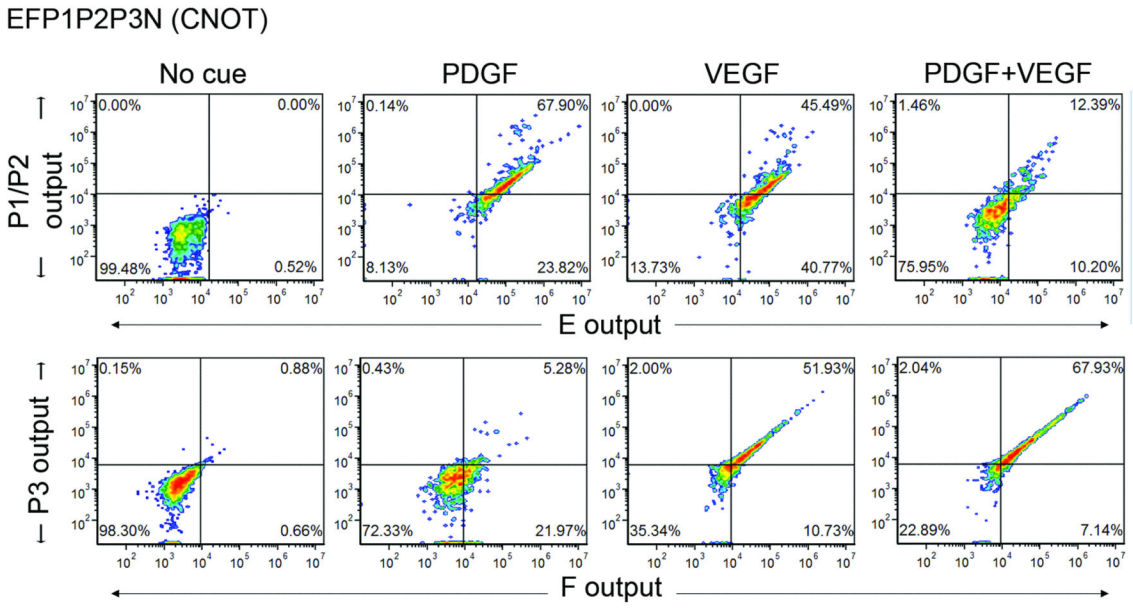

Fig. 3. Robots emulating the reversible CNOT gate in a living animal.

Flow cytometric analysis of *B. discoidalis* cells extracted following injection of the EFP1P2P3N architecture with various key profiles. E robots (FAM-tagged, FL1) and P1/P2 robots (Cy5-tagged, FL4) represent the state of the first bit entering the gate; F robots (Alexa546-tagged, FL2) and P3 robots (Alexa594-tagged, FL3) represent the state of second bit which remains unchanged. Slanting patterns of double-positive labeled cells indicate the presence of EP and FP complexes (Fig. S17). 1,000 hemocytes were collected for each experiment.

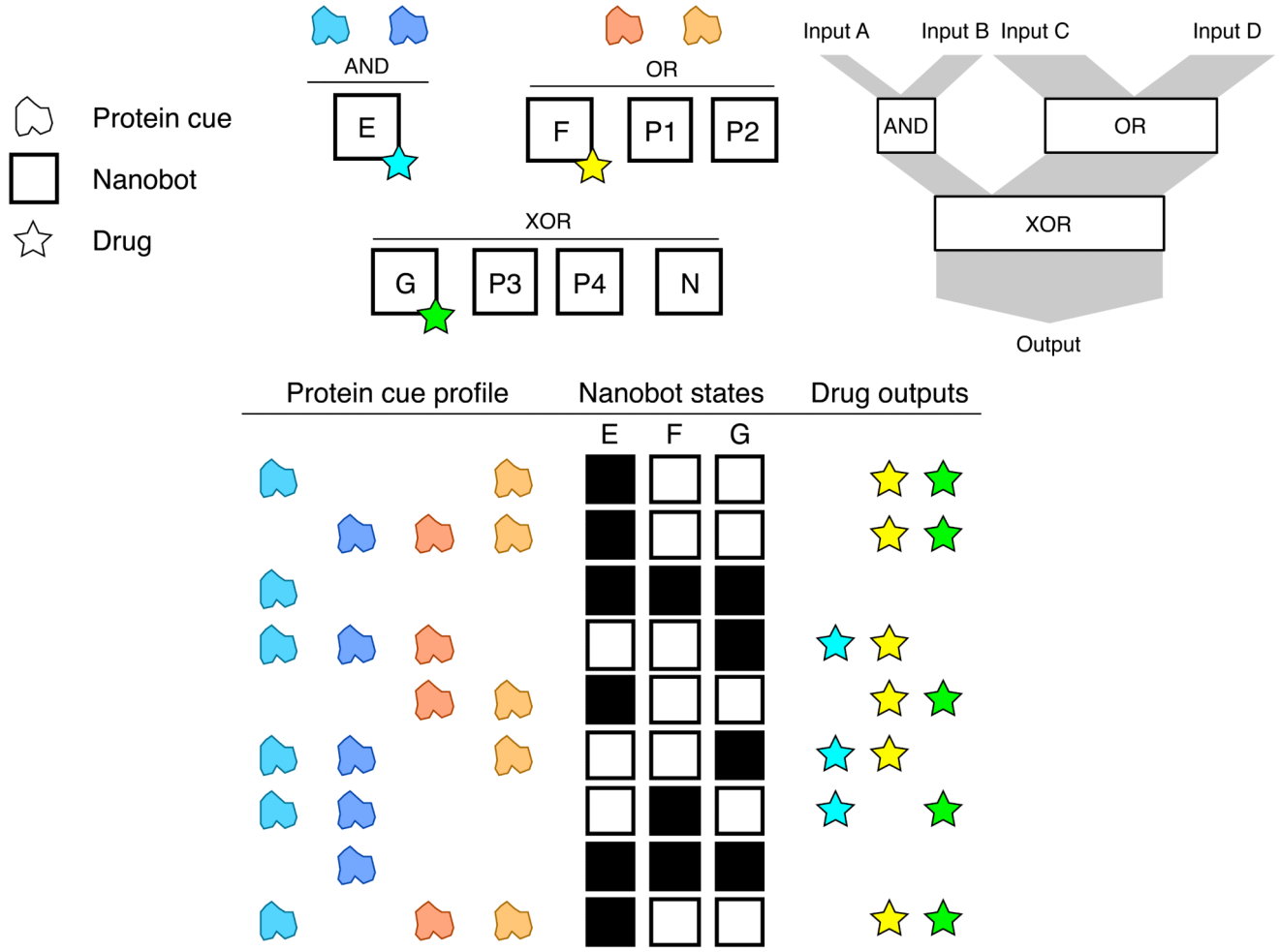

Fig. 4. A hypothetic system capable of simultaneously controlling 3 therapeutic molecules.

This system serves as a processor for an imaginary medical task where a therapeutic response should be tailored per each disease state from a selection of 3 drugs. The system consists of 8 robot types: three effector robots E, F, and G, each carrying a different drug; four positive regulators, P1 and P2 keying F, P3 and P4 keying G; and a negative regulator N inactivating G. Together they form two first layer gates, AND and OR, each controlling its own drug while relaying its output state to a second layer XOR gate, which controls a third drug. This example lists 4 distinct drug combination outputs that could be generated by this system.

Europe PMC Funders Author Manuscripts